



UNIVERSITY OF LEEDS

This is a repository copy of *Carboxylic acids: Effective inhibitors for calcium sulphate precipitation?*.

White Rose Research Online URL for this paper:  
<http://eprints.whiterose.ac.uk/86488/>

Version: Accepted Version

---

**Article:**

Rabizadeh, T, Peacock, CL and Benning, LG (2014) Carboxylic acids: Effective inhibitors for calcium sulphate precipitation? *Mineralogical Magazine*, 78 (6). 1465 - 1472. ISSN 0026-461X

<https://doi.org/10.1180/minmag.2014.078.6.13>

---

**Reuse**

Unless indicated otherwise, fulltext items are protected by copyright with all rights reserved. The copyright exception in section 29 of the Copyright, Designs and Patents Act 1988 allows the making of a single copy solely for the purpose of non-commercial research or private study within the limits of fair dealing. The publisher or other rights-holder may allow further reproduction and re-use of this version - refer to the White Rose Research Online record for this item. Where records identify the publisher as the copyright holder, users can verify any specific terms of use on the publisher's website.

**Takedown**

If you consider content in White Rose Research Online to be in breach of UK law, please notify us by emailing [eprints@whiterose.ac.uk](mailto:eprints@whiterose.ac.uk) including the URL of the record and the reason for the withdrawal request.



[eprints@whiterose.ac.uk](mailto:eprints@whiterose.ac.uk)  
<https://eprints.whiterose.ac.uk/>



## 26 **Introduction**

27 Calcium sulfates are important rock forming minerals that occur in thick evaporitic deposits  
28 throughout geologic history (Kinsman, 1969). In the calcium sulfate system three phases with  
29 various degrees of hydration exist: the dihydrate gypsum ( $\text{CaSO}_4 \cdot 2\text{H}_2\text{O}$ ), the hemihydrate  
30 bassanite ( $\text{CaSO}_4 \cdot 0.5\text{H}_2\text{O}$ ) and the anhydrous anhydrite ( $\text{CaSO}_4$ ). The stability and formation  
31 of these phases are highly temperature and concentration dependent (Freyer and Voigt, 2003).  
32 Between ambient and  $\sim 40^\circ\text{C}$  the most stable phase is gypsum. With increasing ion  
33 concentrations and / or temperature, the solubilities of bassanite and anhydrite decreases and  
34 this leads to gypsum dehydrating and transforming to these less hydrous polymorphs (Freyer  
35 and Voigt, 2003). However, recently, the mechanisms controlling the nucleation and growth  
36 of gypsum from aqueous solutions have gained renewed interest because gypsum likely does  
37 not form directly from solution. One study (Wang et al., 2012) suggested that gypsum forms  
38 through non-classical nucleation via an amorphous calcium sulfate intermediate, while  
39 another study (Van Driessche et al., 2012) suggested that gypsum forms not through  
40 amorphous precursors but through the initial precipitation of nanocrystalline bassanite  
41 particles that self-assemble into larger gypsum crystals through oriented attachment.

42 The gypsum formation pathway is important because among calcium sulfates, gypsum is  
43 mined extensively for use as the crucial component in plasters and cements (e.g., Camarini  
44 and De Mito, 2011), yet to make plasters gypsum has to be dehydrated to bassanite through  
45 the use of large amounts of energy. Equally important however, is the fact that in several  
46 industrial processes that rely on water handling systems (e.g., oil and gas production, water  
47 desalination; Moghaddasi et al., 2006; Rahardianto et al., 2008), the precipitation of calcium  
48 sulfate phases leads to the deposition of minerals on pipes, filters and heat exchangers  
49 (forming mineral scales). Cleaning or removing such mineral scales is costly and undesirable

50 and is affecting efficiency and lifetime of processing technologies (e.g., Mi and Elimelech,  
51 2010).

52 In order to reduce or mitigate calcium sulfate scaling, various simple anti-scaling approaches  
53 have been suggested, the most common being the use of inorganic (e.g.,  $Mg^{2+}$ ; Guan et. al.,  
54 2010) or organic additives (e.g., sulfonic, phosphonic or carboxylic compounds; Shakkthivel  
55 and Vasudevan, 2006; Prisciandaro et al., 2005; Akyol et. al., 2009). The main requirements  
56 for an effective additive are that (a) it is readily available, (b) it is effective at low  
57 concentrations, (c) it is cheap and its addition will not significantly affect production costs,  
58 (d) ideally it is biodegradable or non-toxic to the environment and (e) it reduces mineral  
59 formation or prevents nucleated phases from adhering to surfaces of crucial production  
60 apparatus. Among additives fulfilling many of the above requirements are carboxylic acids  
61 (Hasson et al., 2011; Cao et al., 2014). To date studies that tested the effects of carboxylic  
62 acids on calcium sulfate precipitation have primarily evaluated changes in precipitation onset  
63 or the effect of high temperatures (Prisciandaro et al., 2005; Senthilmurugan et al., 2010;  
64 Ling et al., 2012; Amjad and Koutsoukos, 2014). Still missing is a mechanistic understanding  
65 of the effects of variable concentrations of carboxylic acid and / or various carboxylic acid  
66 moieties.

67 To address this gap we present results on the effects of three carboxylic acids (citric, maleic  
68 and tartaric) and variable additive concentrations (0-20 ppm) on the kinetics and phase  
69 morphologies that develop during homogeneous calcium sulfate formation reactions and  
70 derive a more mechanistic understanding of the processes.

71

## 72 **Experimental methods**

73

74 Inhibitor-free calcium sulfate precipitates (termed ‘pure CaSO<sub>4</sub>’ hereafter) were produced by  
75 mixing equal volumes of a 100 mM CaCl<sub>2</sub>·2H<sub>2</sub>O solution and a 100 mM Na<sub>2</sub>SO<sub>4</sub> solution (99  
76 % purity, VWR) at room temperature (21 °C) and under constant and continuous stirring. The  
77 mixed solutions were supersaturated with respect to gypsum (saturation index SI<sub>Gyp</sub> = 0.5) but  
78 undersaturated with respect to bassanite (SI<sub>Bas</sub> = -0.37). The saturation indices (as the  
79 logarithm of the ion activity product over the solubility product) and the related solubility  
80 products ( $K_{sp,gypsum} = 10^{-3.66}$  and  $K_{sp,bassanite} = 10^{-4.53}$ ) were calculated with the  
81 geochemical computer code PHREEQC using the LLNL database (Parkhurst and Appelo,  
82 1999).

83 Carboxylic acids (citric, maleic or tartaric acid; 99-100 %, VWR) were added to the initial  
84 sodium sulfate solution at concentrations between 5 and 20 ppm. In all experiments, prior to  
85 mixing, the pH of the initial solutions was adjusted to 7, with 0.1 M NaOH.

86 The kinetics of the reactions in the absence and presence of carboxylic acids was monitored  
87 through the development of turbidity in the mixed solutions as measured with a UV-VIS  
88 spectrophotometer (Uvikon XL) at 520 nm. Reactions were followed in triplicate at room  
89 temperatures for up to 4 hours and the variations in the turbidity onset from the three repeats  
90 are reported in minutes. At intermediate time steps and at the end of each experiment the  
91 solutions were quench-filtered (0.2 μm) under vacuum with isopropanol and the solids  
92 retrieved. These solids were characterized for their mineralogy using powder X-ray  
93 diffraction (XRD; Bruker D8 diffractometer; CuKα1; 5-30 °2θ; 0.105 °2θ / step), while the  
94 morphology of the formed phases was imaged using a field emission gun scanning electron  
95 microscope (FEG-SEM, FEI Quanta 650, 3 kV).

96

## 97 **Results**

98

99 Turbidity developed in all experiments but the onset of turbidity occurred after different  
100 elapsed times (induction times) that were dependent on additive type and concentration.  
101 Comparing the turbidity curve from the pure  $\text{CaSO}_4$  experiment with equivalent curves from  
102 experiments where 20 ppm of the 3 carboxylic acids were added (Fig. 1), revealed a  
103 carboxylic acid dependent increase in induction time. In the pure  $\text{CaSO}_4$  system the first  
104 increase in turbidity was observed after  $6\pm 1$  min and the increase in absorbance took ~ 60  
105 minutes to reach a steady value on a plateau. In the presence of 20 ppm carboxylic acids the  
106 induction times increased to  $9\pm 1$  min,  $16\pm 1$  min and  $25\pm 1$  min for tartaric, maleic acid and  
107 citric acid, respectively, and specifically in the case of added citric acid the reaction curve  
108 took much longer to reach a plateau (~ 200 min; Fig. 1).

109

110 (Insert Fig. 1 here)

111

112 Testing variable concentrations of citric acid (5, 10, 20 ppm) showed a proportional increase  
113 in induction time with increasing additive concentration (Fig. 2). The  $6\pm 1$  minute induction  
114 time observed in the pure  $\text{CaSO}_4$  system almost doubled in the presence of 5 ppm citric acid  
115 ( $10\pm 1$  minutes), tripled with 10 ppm ( $17\pm 1$  minutes) and at 20 ppm citric acid added an  
116 induction time 4 times greater than that in the pure  $\text{CaSO}_4$  system was observed ( $25\pm 1$   
117 minutes).

118

119 (Insert Fig. 2 here)

120

121 XRD analyses of the solids recovered at the end of each reaction (in both the pure and  
122 carboxylic acid amended experiments) revealed that the sole mineral end product was  
123 gypsum. However, samples filter-quenched just after the onset of turbidity in the pure and  
124 citric acid system (e.g., after 30 sec in the pure system and after 3 and 10 min in the presence  
125 of 20 ppm citric acid; marked with \* in Fig. 2 and corresponding to ~ 7, 26 and 35 minutes in  
126 absolute time respectively) showed in the XRD patterns the presence of bassanite coexisting  
127 with gypsum (Fig. 3a,c). In both cases with time, the proportion of bassanite decreased  
128 (bassanite peaks decreased in intensity or fully disappeared) showing that bassanite was an  
129 intermediate phase (Fig. 3d) but that in both systems the final product was pure gypsum (Fig.  
130 3b,e). As mentioned above, an increase in induction time prior to the onset of turbidity was  
131 also observed in the presence of the other two carboxylic acids (maleic and tartaric; Fig. 1).  
132 Although the shape and slope of the turbidity curves hint at a similar process, we do not have  
133 equivalent time resolved XRD evidence that these additives also stabilized bassanite (but see  
134 below and Fig. 4 e,f).

135

136 (Insert Fig. 3 here)

137

138 Photomicrographs of the intermediate (~ 7 minutes, or 30 seconds after onset of turbidity)  
139 and end product (after 70 minutes of total reaction) materials in the pure CaSO<sub>4</sub> system  
140 revealed bassanite present at the beginning of the reaction only as elongated nanorods (up to  
141 ~ 200 nm long) while at the end of the experiment only gypsum was present as larger (~ up to  
142 μm size), thin, needle-like crystals, in part twinned (Fig. 4a and b). These morphologies and  
143 sizes are equivalent with those reported by Van Driessche et al. (2012) and Wang et al.  
144 (2013) and the presence of bassanite in our samples had already been documented through

145 XRD (Fig. 3a,c). At the end of the pure system crystallization reaction (Fig. 4b) all bassanite  
146 had transformed and only large, elongated (between 5-50  $\mu\text{m}$ ) needle-like and twinned  
147 gypsum crystals were present, again confirming the XRD data (Fig. 3b). In the presence of 20  
148 ppm citric acid, after the onset of turbidity (3 minutes = 28 minutes after mixing of the initial  
149 solutions) the bassanite identified by XRD (Fig. 3c) was present as very small but almost  
150 isometric nanoparticles ( $< \sim 90 \text{ nm}$ ; Fig. 4c) that occurred together with larger gypsum  
151 crystals. At the end of the reaction when the turbidity curve reached a plateau (after 200  
152 minutes; Fig. 4d) only gypsum was present. It was striking that, compared to the pure  $\text{CaSO}_4$   
153 system both the bassanite and gypsum in the citrate system did not exhibit the typical  
154 bassanite nanorod or gypsum needle-like habits, but rather far more isometric (bassanite; Fig.  
155 4c) and distinctly platy (gypsum; Fig. 4d) habits. Although we have no XRD evidence of  
156 bassanite stabilization in the presence of maleic and tartaric acid, photomicrographs of  
157 samples removed a few minutes after the onset of turbidity in the 20 ppm experiments with  
158 these carboxylic acids present revealed equivalent nanorod (particles  $< 200 \text{ nm}$ )  
159 morphologies that we infer to be bassanite. These occurred together with longer needle-like  
160 crystals inferred to be gypsum (Fig. 4e and f). In contrary to the citric acid system however,  
161 in the presence of 20 ppm tartaric or maleic acid the shape, size or habit of the intermediate  
162 bassanite and end product gypsum were the same as in the pure  $\text{CaSO}_4$  experiment, although  
163 a slight ‘thinning’ of the gypsum needles was observed.

164

165 (Insert Fig. 4 here)

166

167 **Discussion**

168

169 Measuring turbidity and estimating induction times in the absence and presence of additives  
170 is one of the most common methods of evaluating the efficiency of additives as a mechanism  
171 to delay the nucleation and growth of sparingly soluble scale minerals.

172 Additives that are biodegradable, like the carboxylic acids used in the current study, and that  
173 also dramatically delay the nucleation and or growth of a phase at low concentrations, are  
174 considered effective and are often called ‘inhibitors’ although they do not inhibit nucleation  
175 and growth but most often just delay or change the reaction progress.

176 Our data revealed that at equal concentrations (20 ppm), among the three additives tested,  
177 citric acid increased the induction time and decreased the slope of the turbidity curve more  
178 than both the tartaric and maleic acid, inferring that citric acid is inherently a better inhibitor.

179 If we also consider the differences in molar concentrations of the used carboxylic acids  
180 ( $C_{\text{cit}} = 1.01 \mu\text{M}$ ,  $C_{\text{tart}} = 1.33 \mu\text{M}$  vs.  $C_{\text{mal}} = 1.72 \mu\text{M}$ ) further supports the fact that citric acid  
181 is the most effective inhibitor despite it being present in the lowest molar concentration.

182 However, the exact reasons for its higher effectiveness are not yet clear but likely also stem  
183 from the variations in molecular geometries and sorption capacities between these three  
184 carboxylic acids.

185 It is well known that additives can affect the nucleation and growth of scale minerals, for  
186 example, by forming complexes or chelating agents with the active ions in the nucleating  
187 solutions (eq. 1; where  $x = 2$  for maleic / tartaric acids or 3 for citric acid) or by sorbing to  
188 active crystal sites and inhibiting mineral growth (e.g., Crabtree et al., 1999; Badens et al.,  
189 1999; Ersen et al., 2006; Magallanes-Rivera et al., 2009).

190



192

193 In the case of the carboxylic acids tested, complexation with calcium is well known (Bazin et  
194 al., 1995) but sorption and growth inhibition also seems to play an important role. All  
195 carboxylic acids delayed the onset of nucleation (increased induction time compared to pure  
196 system, Fig.1 and 2). However, the citric acid additive also affected the growth of the scale  
197 mineral in that both bassanite and gypsum exhibited different habits compared to the additive  
198 free phases (Fig. 4). Finally, of interest for mineral scale formation and inhibition is the fact  
199 that compared to the pure system even low concentrations of citric acid stabilized the  
200 bassanite phase for much longer periods.

201 In additive experiments one of the fundamental parameters that controls ‘inhibition’ either  
202 through complexation with the active ions (in this case  $\text{Ca}^{2+}$ ) or sorption to active growth  
203 sites is the speciation and degree of protonation of the additive used. All our experiments  
204 with or without additives were carried out with the initial solutions adjusted to pH 7. At this  
205 pH value all carboxylic acids are to the largest extent deprotonated (Table 1).

206

207 (Insert Table 1 here)

208

209 The delay in precipitation, indicated by the increased induction time, is likely in part due to  
210  $\text{Ca}^{2+}$  complexation with these deprotonated species through the reduction of  $\text{Ca}^{2+}$   
211 supersaturation. Of the carboxylic acids tested, citric acid at pH 7 is the most deprotonated  
212 and maybe therefore it acts as the most efficient inhibitor, as reflected in the longest induction  
213 time. Nevertheless, the nucleation barrier in the presence of all additives is overcome and  
214 bassanite nucleates and eventually transforms to gypsum. The delay in precipitation in the  
215 presence of the carboxylic acid may also be attributed to sorption onto bassanite and gypsum  
216 growth sites. Badens et al. (1999) and Ersen et al. (2006) found that adsorption of citrate onto

217 active growth faces of both bassanite and gypsum inhibited growth in those directions more  
218 than other carboxylic acid (e.g., tartaric or malic). This suggests that with citric acid both  
219 bassanite and gypsum grew with different habits from those in the pure  $\text{CaSO}_4$  system, as our  
220 imaging data also confirmed (Fig. 4a,b). Citric acid seems to have inhibited growth along the  
221 c axis and prevented the formation of typical long, needle-like habits. Instead, the growth of  
222 gypsum was favoured in the a and b directions, leading to platy crystal habits (Fig. 4).  
223 Similar morphological changes in gypsum habits in the presence of carboxylic acids have  
224 been reported by others (Li et al., 2007; Magallanes-Rivera et al., 2009), yet a molecular level  
225 understanding of the process is still lacking.

226 For gypsum formed in the presence of citric acid Prisciandaro et al. (2005) showed that the  
227 increase in induction time was due to a dramatic change in interfacial tension compared to an  
228 additive free system. Although our work confirmed these findings, we also showed that  
229 bassanite is a metastable intermediate forming prior to gypsum not just in the pure  $\text{CaSO}_4$   
230 system (Wang et al., 2012; Van Driessche et al., 2012) but also in the presence of carboxylic  
231 acids. In the pure system, bassanite forms below its thermodynamic bulk solubility and its  
232 transformation to gypsum is through hydration and self-assembly via a process controlled by  
233 a particle size dependent surface energy (Van Driessche et al., 2012). This is different to the  
234 non-classical nucleation, growth and dehydration pathways suggested for calcium carbonates  
235 (Rodriguez Blanco et al., 2011; Bots et al., 2012) or calcium phosphates (Combes and Rey,  
236 2010). However, the current study shows that in the presence of even low concentrations of  
237 carboxylic acid, (a) the onset of the precipitation reaction is delayed, (b) bassanite is  
238 stabilized and its transformation to gypsum slowed down, and (c) citric acid changes the  
239 shape and habit of the formed bassanite and gypsum.

240 Thus, if citric acid inhibitors are used in an industrial fluid handling system (where  $\text{CaSO}_4$   
241 scale minerals are a problem), they can substantially retard nucleation and growth even at low

242 concentrations. Importantly, citric acid may not just stabilize a nanoparticulate phase like  
243 bassanite and thus reduce clogging of filters, but the size effect may also prevent adherence to  
244 pipe surfaces. However, this latter process and further growth of CaSO<sub>4</sub> phases on surfaces is  
245 still under study.

246

## 247 **Acknowledgements**

248

249 This study was supported by the Marie Curie grant from the European Commission in the  
250 framework of the MINSC ITN (Initial Training Research network), Project number 290040.

251 The authors would like to thank the Cohen Laboratories in the School of Earth and  
252 Environment, and the Leeds Electron Microscopy and Spectroscopy Centre (LEMAS) for  
253 help and access to instruments during the course of this study. We would like to also thank  
254 three reviewers and the associate editor for their constructive comments, which helped  
255 improve our paper.

256

## 257 **References:**

258

259 Akyol, E., Oner, M., Barouda, E., and Demadis, K.D. (2009) Systematic structural  
260 determinants of the effects of tetraphosphonates on gypsum crystallization. *Crystal*  
261 *Growth & Design*, **9**, 5145-5154.

262 Amjad, Z. and Koutsoukos, P.G. (2014) Evaluation of maleic acid based polymers as scale  
263 inhibitors and dispersants for industrial water applications. *Desalination*, **335**, 55-63.

264 Badens, E., Veessler, S., and Boistelle, R. (1999) Crystallization of gypsum from hemihydrate  
265 in presence of additives. *Journal of crystal growth*, **198**, 704-709.

266 Bazin, H., Bouchu, A., Descotes, G. and Petit-Ramel, M. (1995) Comparison of calcium  
267 complexation of some carboxylic acids derived from D-glucose and D-fructose. *Canadian*  
268 *Journal of Chemistry*, **73**, 1338-1347.

269 Bots, P., Rodriguez-Blanco, J.D., Roncal-Herrero, H., Shaw, S. and Benning, L. (2012)  
270 Mechanistic insights into the crystallization of amorphous calcium carbonate (ACC).  
271 *Crystal Growth & Design*, **12**, 3806-3814.

272 Camarini, G. and De Milito, J.A. (2011) Gypsum hemihydrate–cement blends to improve  
273 renderings durability. *Construction and Building Materials*, **25**, 4121-4125.

274 Cao, K., Zhou, Y., Liu, G., Wang, H. and Sun, W. (2014) Preparation and Properties of a  
275 Polyether-Based Polycarboxylate as an Antiscalant for Gypsum. *Journal of applied*  
276 *polymer science*, **131**, 1-9.

277 Combes, C. and Rey, C. (2010) Amorphous calcium phosphates: synthesis, properties and  
278 uses in biomaterials. *Acta Biomaterialia*, **6**, 3362–3378.

279 Crabtree, M., Slinger, D., Fletcher, P., Miller, M., Johnson, A. and King, G. (1999) Fighting  
280 scale—removal and prevention. *Oilfield Review*, **11**, 30-45.

281 Ersen, A., Smith, A., and Chotard, T. (2006) Effect of malic and citric acid on the  
282 crystallisation of gypsum investigated by coupled acoustic emission and electrical  
283 conductivity techniques. *Journal of materials science*, **41**, 7210-7217.

284 Freyer, D. and Voigt, W. (2003) Crystallization and phase stability of CaSO<sub>4</sub> and CaSO<sub>4</sub>–  
285 based salts. *Monatshefte für Chemie/Chemical Monthly*, **134**, 693-719.

286 Guan, B., Yang, L., and Wu, Z. (2010) Effect of Mg<sup>2+</sup> ions on the nucleation kinetics of  
287 calcium sulfate in concentrated calcium chloride solutions. *Industrial & Engineering*  
288 *Chemistry Research*, **49**, 5569-5574.

289 Hasson, D., Shemer, H. and Sher, A. (2011) State of the Art of Friendly “Green” Scale  
290 Control Inhibitors: A Review Article. *Industrial & Engineering Chemistry Research*, **50**,  
291 7601-7607.

292 Kinsman, D.J. (1969) Modes of Formation, Sedimentary Associations, and Diagnostic  
293 Features of Shallow-Water and Supratidal Evaporites. *The American Association of*  
294 *Petroleum Geologists Bulletin*, **53**, 830-840.

295 Li, J., Li, G., and Yu, Y. (2007) The influences of gypsum water-proofing additive on  
296 gypsum crystal growth. *Materials letters*, **61**, 872-876.

297 Lide, D. R. (Ed.). (1988) *CRC handbook of chemistry and physics*. CRC press , **88**, chapter 8  
298 page 49.

299 Ling, L., Zhou, Y., Huang, J., Yao, Q., Liu, G., Zhang, P., Sun, W. and Wu, W. (2012)  
300 Carboxylate-terminated double-hydrophilic block copolymer as an effective and  
301 environmental inhibitor in cooling water systems. *Desalination*, **304**, 33-40.

302 Magallanes-Rivera, R.X., Escalante-Garcia, J.I., and Gorokhovskiy, A. (2009) Hydration  
303 reactions and microstructural characteristics of hemihydrate with citric and malic acid.  
304 *Construction and Building Materials*, **23**, 1298-1305.

305 Mi, B. and Elimelech, M. (2010) Gypsum Scaling and Cleaning in Forward Osmosis:  
306 Measurements and Mechanisms. *Environmental science and technology*, **44**, 2022-2028.

307 Moghadasi, J., Sharif, A., Müller-Steinhagen, H. and Jamialahmadi, M. (2006) Prediction of  
308 scale formation problems in oil reservoirs and production equipment due to injection of  
309 incompatible waters. *Developments in Chemical Engineering and Mineral Processing*, **14**,  
310 545-566.

311 Parkhurst, D.L., and Appelo, C.A.J. (1999) User's guide to PHREEQC (Version 2): A  
312 computer program for speciation, batch-reaction, one-dimensional transport, and

313 inverse geochemical calculations. US Geological Survey Water Resource Investigation.  
314 Report 99-4259, 312p.

315 Prisciandaro, M., Santucci, A., Lancia, A. and Musmarra, D., (2005) Role of citric acid in  
316 delaying gypsum precipitation. *The Canadian Journal of Chemical Engineering*, **83**, 586-  
317 592.

318 Rodriguez-Blanco, J.D., Shaw, S. and Benning, L.G. (2011) The kinetics and mechanisms of  
319 amorphous calcium carbonate (ACC) crystallization to calcite, via vaterite. *Nanoscale*, **3**,  
320 265-271.

321 Rahardianto, A., Mccool, C.B. and Cohen, Y. (2008) Reverse osmosis desalting of inland  
322 brackish water of high gypsum scaling propensity: kinetics and mitigation of membrane  
323 mineral scaling. *Environmental science and technology*, **42**, 4292–4297.

324 Senthilmurugan, B., Ghosh, B., Kundu, S.S., Haroun, M. and Kameshwari, B. (2010) Maleic  
325 acid based scale inhibitors for calcium sulfate scale inhibition in high temperature  
326 application. *Journal of Petroleum Science and Engineering*, **75**, 189-195.

327 Shakkthivel, P., and Vasudevan. T. (2006) Acrylic acid-diphenylamine sulphonic acid  
328 copolymer threshold inhibitor for sulphate and carbonate scales in cooling water systems.  
329 *Desalination*, **197**, 179-189.

330 Van Driessche, A.E.S., Benning, L.G., Rodriguez-Blanco, J.D., Ossorio, M., Bots, P. and  
331 Garcia-Ruiz, J.M. (2012) The role and implications of bassanite as a stable precursor  
332 phase to gypsum precipitation. *Science*, **336**, 69-72.

333 Wang, Y.W., Kim, Y.Y., Christensonb, H.K. and Meldrum, F.C. (2012) A new precipitation  
334 pathway for calcium sulfate dihydrate (gypsum) via amorphous and hemihydrate  
335 intermediates. *Chemical Communications*, **48**, 504-506.

336 Wang, Y.W., Christenson, H.K., and Meldrum, F.C. (2013) Confinement leads to control  
337 over calcium sulfate polymorph. *Advanced Functional Materials*, **23**, 5615-5623.



339 **Table: Rabidazeh et al:**

340

341 Table 1. Dissociation constants of carboxylic acids used (from Lide, 1988)

<b>Carboxylic acid moiety</b>	<b>pK<sub>a1</sub></b>	<b>pK<sub>a2</sub></b>	<b>pK<sub>a3</sub></b>
Citric acid	3.13	4.76	6.40
Maleic acid	1.92	6.23	
Tartaric acid	3.03	4.34	

342

343

344

345 **Figures Rabidazeh et al:**

346 Fig. 1. The effect of adding 20 ppm tartaric, maleic or citric acid on the development of  
347 turbidity compared to the pure CaSO<sub>4</sub> system.

348 Fig. 2. The effect of variable concentrations of citric acid (5, 10, 20 ppm) on the development  
349 of turbidity; marked with \* are the absolute times (~ 7 minutes in the pure system and 28 and  
350 35 minutes respectively in the 20 ppm citric acid system) when solids were removed and  
351 analysed and data is shown in Fig. 3a, c and d and 4 a and c.

352 Fig. 3. XRD patterns of precipitated materials from (a) the pure CaSO<sub>4</sub> system removed from  
353 the reaction solution 30 seconds after turbidity onset (absolute time is ~ 7 minutes) with stars  
354 marking bassanite peaks of low intensity that are better visible in the insets, where the low  
355 intensity (101) and (400) bassanite peaks are highlighted; (b) same system but 63 minutes  
356 after turbidity onset (absolute time 70 minutes) when the transformation to gypsum was  
357 complete and no bassanite remained; (c-e) XRD patterns from the system with 20 ppm citric  
358 acid added; (c) 3 minutes after turbidity onset (absolute time 28 minutes) showing all four  
359 distinct and very intense bassanite peaks ((101), (200), (301) and (400) all marked with a  
360 star); (d) 10 minutes after turbidity onset (absolute time 35 minutes) showing smaller  
361 bassanite peaks; and (e) 175 minutes after turbidity onset (absolute time 200 minutes) where  
362 only gypsum peaks remain and all bassanite has been transformed.

363 Fig. 4. SEM micrograph of precipitated materials from experiments in (a) the pure CaSO<sub>4</sub>  
364 system 30 seconds after turbidity onset showing bassanite nanorods and gypsum needles; (b)  
365 the pure CaSO<sub>4</sub> system 63 minutes after turbidity onset (= 70 minutes total time) showing  
366 only variably sized gypsum needles; (c) tiny bassanite nanoparticles formed in the presence  
367 of 20 ppm citric acid 3 minutes after turbidity onset together with some larger gypsum  
368 crystals; (d) plate like gypsum crystals formed in the presence of 20 ppm citric acid after 200  
369 minutes of total reaction; (e) bassanite nanorods and single larger gypsum needle collected a

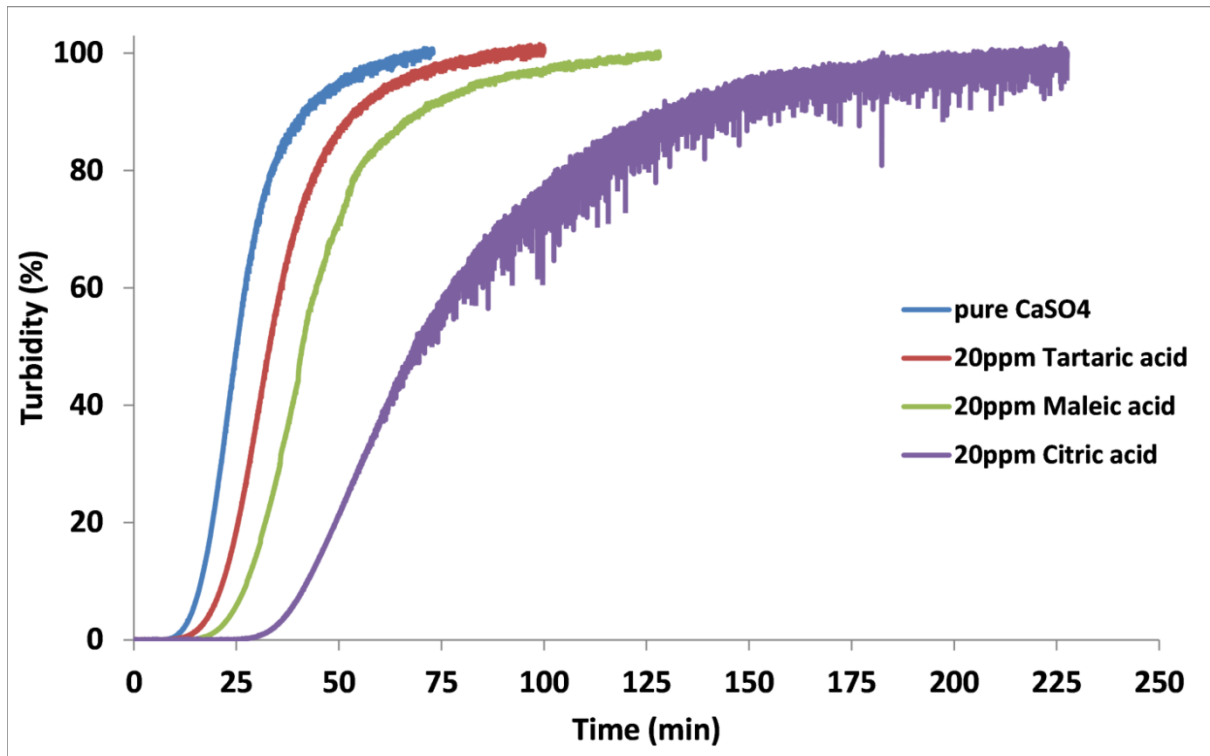
370 few minutes after the onset of turbidity in the 20 ppm maleic acid experiment; (f) bassanite  
371 nanorods and single larger gypsum needle collected a few minutes after the onset of turbidity  
372 in the 20 ppm tartaric acid experiment.

373

374

375

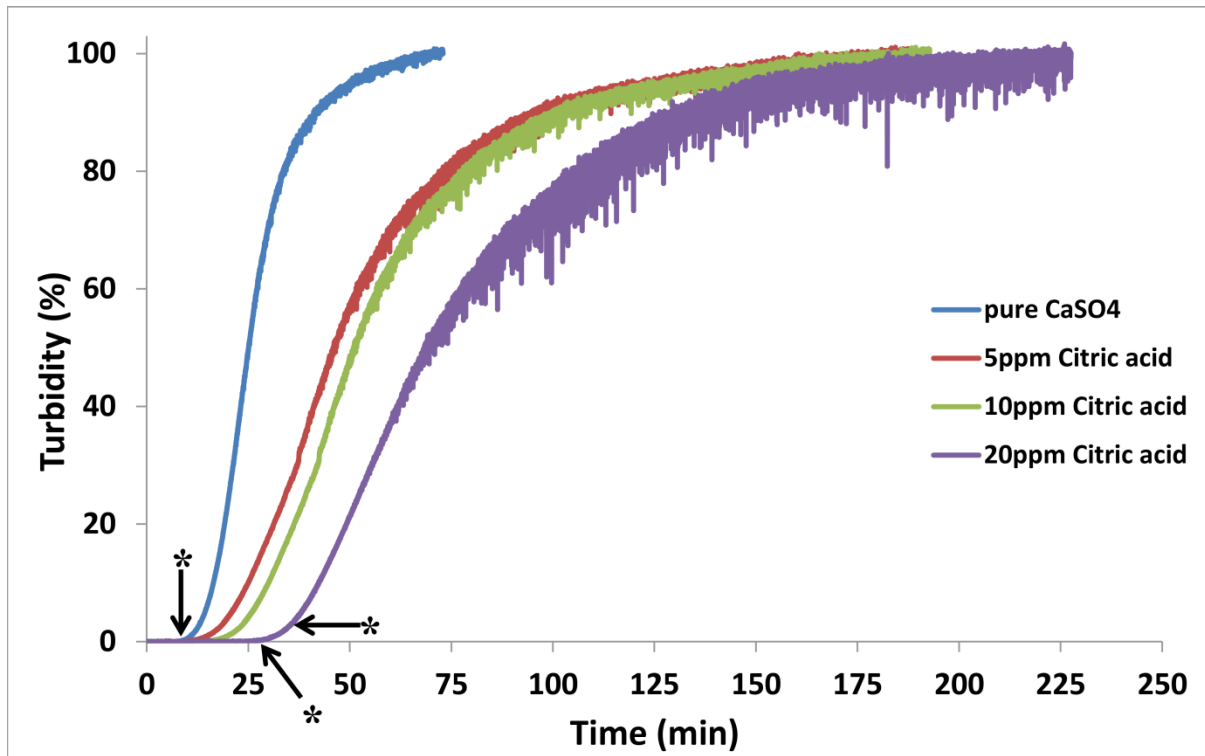
376



378

379  
380  
381

Fig. 1. The effect of adding 20 ppm tartaric, maleic or citric acid on the development of turbidity compared to the pure CaSO<sub>4</sub> system.



383

384 Fig. 2. The effect of variable concentrations of citric acid (5, 10, 20 ppm) on the development of turbidity;  
385 marked with \* are the absolute times (~ 7 minutes in the pure system and 28 and 35 minutes respectively in the  
386 20 ppm citric acid system) when solids were removed and analysed and data is shown in Fig. 3a, c and d and 4 a  
387 and c.  
388

389

390

391

392

393

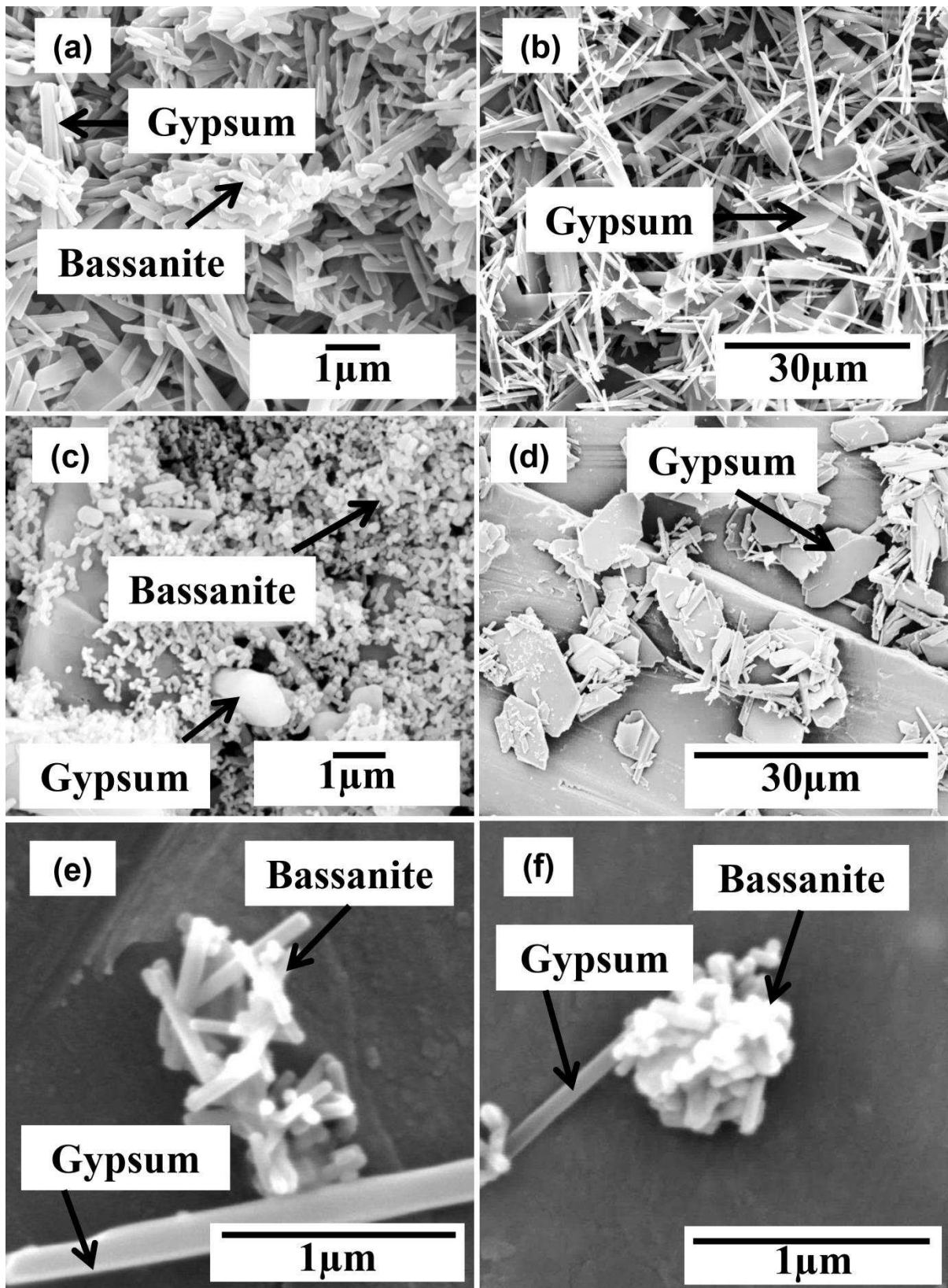
394

395

396



400  
401 Fig. 3. XRD patterns of precipitated materials from (a) the pure  $\text{CaSO}_4$  system removed from the reaction  
402 solution 30 seconds after turbidity onset (absolute time is  $\sim 7$  minutes) with stars marking bassanite peaks of  
403 low intensity that are better visible in the insets, where the low intensity (101) and (400) bassanite peaks are  
404 highlighted; (b) same system but 63 minutes after turbidity onset (absolute time 70 minutes) when the  
405 transformation to gypsum was complete and no bassanite remained; (c-e) XRD patterns from the system with 20  
406 ppm citric acid added; (c) 3 minutes after turbidity onset (absolute time 28 minutes) showing all 3 distinct and  
407 very intense bassanite peaks ((101), (200), (301) and (400) all marked with a star); (d) 10 minutes after turbidity  
408 onset (absolute time 35 minutes) showing smaller bassanite peaks; and (e) 175 minutes after turbidity onset  
409 (absolute time 200 minutes) where only gypsum peaks remain and all bassanite has been transformed.



411

412  
413

Fig. 4. SEM micrograph of precipitated materials from experiments in (a) the pure  $\text{CaSO}_4$  system 30 seconds after turbidity onset showing bassanite nanorods and gypsum needles; (b) the pure  $\text{CaSO}_4$  system 63 minutes

414 after turbidity onset (= 70 minutes total time) showing only variably sized gypsum needles; (c) tiny bassanite  
415 nanoparticles formed in the presence of 20 ppm citric acid 3 minutes after turbidity onset together with some  
416 larger gypsum crystals; (d) plate like gypsum crystals formed in the presence of 20 ppm citric acid after 200  
417 minutes of total reaction; (e) bassanite nanorods and single larger gypsum needle collected a few minutes after  
418 the onset of turbidity in the 20 ppm maleic acid experiment; (f) bassanite nanorods and single larger gypsum  
419 needle collected a few minutes after the onset of turbidity in the 20 ppm tartaric acid experiment.

420

421

422

423

424